Arabian Journal of Geosciences (2023) 16:311
https://doi.org/10.1007/s12517-023-11355-8

ORIGINAL PAPER

An example of artificial neural networks modeling the distribution of mercury (Hg), which poses a risk to human health in the selection of settlements: Sarayönü (Türkiye)

Andaç Batur Çolak[1] · Bilgehan Yabgu Horasan[2] · Alican Öztürk[3] · Mustafa Bayrak[4]

Received: 18 November 2022 / Accepted: 9 March 2023 / Published online: 14 April 2023

Abstract
As part of this research, the Ladik-Sarayönü area of Konya province's air quality has been assessed utilizing an AI (Artificial Intelligence) method. A total of 103 field samples were analyzed experimentally. Data from experiments was used to inform the design of a multi-layer perceptron feed-forward back-propagation artificial neural network model. The Bayesian method has been employed as the training procedure in an artificial neural network model with 15 neurons in its hidden layer. One hundred experimental data points were used to develop a network model that predicts mercury values of the geoaccumulation index value in the output layer based on the following input variables: mercury, distance to the pollution source, source of pollution, characteristics of the sampled place and the primary factor that controls moving parameters. The majority (90%) of the data is used for the model's training process, while the remaining (10%) is used for validation. By comparing the model's anticipated outcomes with experimental data, an artificial neural network was used to evaluate the model's prediction performance. To forecast mercury values of the geoaccumulation index, the created artificial neural network had an error rate of −4.04 to 3.98% (with an average of −0.58%). The MSE for the network model is 2.1×10^{-1}, and the R value is 0.9533.

Keywords Heavy metal · Mercury · Artificial neural network · Bayesian algorithm · Konya

Introduction

Rapid increase in world population and agriculture, mining and increasing industrial production activities caused serious problems in environmental pollution. Mining activities on the lands near the areas where mining activities are carried out cause serious environmental effects, and these effects cause permanent toxicological problems for the environment even after centuries (Khalil et al. 2013). Heavy commodities dispersed due to these activities are a global threat, and mercury, long-range atmospheric portability, permanence, toxicity and bioaccumulative properties are a global problem (Cheng et al. 2013). The presence of metal such as mercury (Hg) in soils and agricultural areas poses an important threat to human health (Tóth et al. 2016; Sierra et al. 2017). In biological systems, Hg is a non-essential element; therefore, there are generally no dedicated pathways for its metabolization and/or excretion. As a result, Hg bioaccumulates and grows throughout the food chain. It is organic and inorganic forms of mercury. Methylmercury is a particularly serious problem; it can accumulate in foods at high biological concentrations and is known to cause neurological, nephrological and immunological diseases in humans (Tiodar Emanuela et al. 2021). Moreover, elemental Hg and its various compounds are highly volatile, providing a bi-directional exchange between soil and atmosphere (i.e. accumulation and evaporation) (Kim and Lindberg 1995; Fu et al. 2015). Soil represents a potential source and begins in the Hg cycle. Their inclusion in metal food nets in the soils is an easy

Responsible Editor: Amjad Kallel

✉ Andaç Batur Çolak
abcolak@ticaret.edu.tr

[1] Information Technologies Application and Research Center, Istanbul Ticaret University, 34445 Istanbul, Türkiye

[2] Department of Environmental Protection and Technologies, Selcuk University Sarayönü Vocational School of Higher Education, Sarayönü/Konya, Türkiye

[3] Department of Geological Engineering, Faculty of Engineering and Natural Sciences, Konya Technical University, Selçuklu/Konya, Türkiye

[4] Department of Mechanical Engineering, Engineering Faculty, Niğde Ömer Halisdemir University, Niğde, Türkiye

way to transition to people (Gall et al. 2015). Heavy metals such as mercury and arsenic can remain in the soil for many years (Ozturk and Arici 2021). Heavy metals can be carried away from their locations by stream sediments and can form accumulations (Solgun et al. 2021). Plants such as vegetables can be a direct way for people to be exposed to metals (Manwani et al 2022). Therefore, it is necessary to know the size and distribution of heavy metal concentration in the soil. Heavy metal accumulations are not only caused by anthropogenic processes, they can also occur as a result of geogenic processes (Coskun et al. 2021). Heavy metal accumulations due to geogenic factors are distributed over wide areas. Therefore, estimating the size of anthropogenic distributions may be easier than estimating distributions of geonenic origin. It is of great importance for human health to be able to estimate the effect of pollution occurring in large areas with the right parameters in a short time. Due to the negative effects of studies on pollution analysis such as cost and time, the importance of predictive studies has increased. A limited number of studies have been conducted in the literature to estimate environmental and soil pollution by artificial intelligence tools (Akinpelu et al. 2020; Bazoobandi et al. 2019; Nourani et al. 2020; Emamgholizadeh et al. 2018). Artificial intelligence-based forecasting methods are popular applications that have been found in many fields by researchers recently. Artificial neural networks stand out among the tools frequently used by researchers in modeling and simulating nonlinear complex functions (Bahiraei et al. 2019). Moosavi et al. (2012) used multi-output least squares support vector regression for simultaneous estimation of interpore flow coefficient and storage rate. In the study, 500 pressure transient response databases for horizontal wells in naturally fragmented reservoirs were generated by the finite element method, converted to pressure derivative curves and then used to develop and evaluate this automated characterization paradigm. The predictive accuracy of the model has been checked and verified by both soft and noisy pressure transient responses. The proposed model was able to predict the storage rate and the interpore flow coefficient with overall absolute mean relative deviations of 0.186% and 3.754%, respectively. Correlation coefficients of 1 and 0.99992 were obtained for the estimation of the storage rate and the interpore flow coefficient, respectively. The leverage outlier detection technique confirmed that only less than 6% of the predictions were within the suspect zone.

Ladik (Konya) history is quite old, and it was a settlement located at an important road junction in the east of the Roma. The region has been an important mining region since the Roman empire. Mercury ovens, which have been operated many times until today, have been closed with the loss of economic value in the 1990s. In addition, the Ladik-Sarayonu (Konya) connection road has a very old history and has been actively used for hundreds of years. The region is exposed to anthropogenic and geogenic mercury pollution for a long time due to the mercury companies operating for a very long time. In this study, an artificial neural network was developed to estimate the pollution level of the settlements and agricultural areas in the Ladik-Sarayönü region. The simulation values obtained using the artificial neural network developed with a total of 103 experimental data obtained from three different data sets were compared with the experimentally obtained pollution values, and the estimation performance of the artificial neural network was analyzed. As can be seen from the comprehensive literature review, there is no research for estimating the pollution values related to mercury concentration with artificial neural network. This study is very important since it aims to fill the gap in this field in the literature.

Material and methods

In this study, a simulation model has been developed in order to estimate the mercury pollution on the settlement and agricultural areas of the mercury enterprise located at the borders of Ladik-Sarayönü with an artificial intelligence approach. In the study, the geoaccumulation index values obtained for the mercury in the studies of abandoned mercury in Ladik settlement and agricultural areas and heavy metal accumulation in the agricultural areas on the Ladik-Sarayönü connection road were used (Horasan et al. 2020). The map of the study area is given in Fig. 1. The geoaccumulation index values were calculated using Eq. (1) and mercury concentrations obtained from the chemical analysis of a total of 103 samples taken from the field (Muller 1969).

$$I_{\text{geo}} = \left[\frac{C_n}{1.5 \times B_n}\right] \tag{1}$$

Here C_n is the heavy metal concentration measured in the precipitate and B_n is the geochemical background value in the schist of the average elements. Factor 1.5 is used for possible variations of background data depending on the lithological variations (Srinivasa et al. 2019).

In order to analyze the HgI_{geo} value, 103 different samples were taken from the study area, and a comprehensive evaluation was made with a total of 103 experimental data. During the sampling process, the first 1–2-cm depth of the ground was cleaned, and 5-kg sample was taken from 20-cm depth. The samples taken were kept in the oven at 60 °C for 24 h and dried. The dried samples were ground after crushing using a plastic mallet, and the particle size was reduced to − 80 mesh. These obtained samples were again turned into 300-g packs and kept as witness samples. Mercury

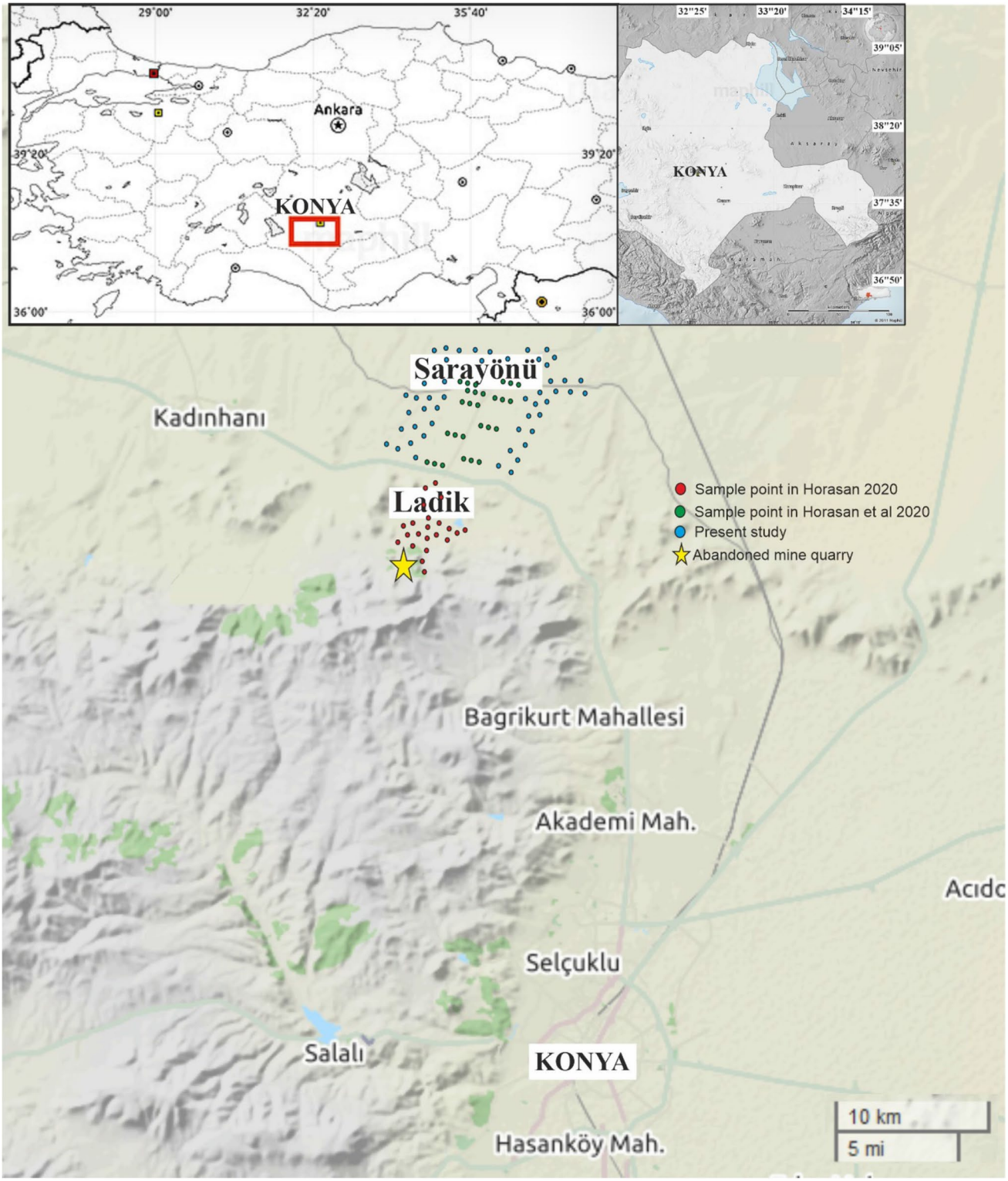

Fig. 1 The map of the study area

concentration was determined by giving the solution sample prepared for Perkin Elmer Inductively Coupled Plasma-Mass Spectrometer (ICP-MS) device.

Due to the time losses and financial disadvantages of the experimental studies, there are many studies and different methodologies that were conducted to estimate the results

by processing data (Gao et al. 2018, 2019). Modeling of irregular traditional estimation algorithms is insufficient in estimating time-related irregular data or complex nonlinear functions (Bahiraei et al. 2019). Information on the mercury concentration and location of the study area is presented in Tables 1, 2, and 3.

ANN model development

One of the most popular artificial intelligence applications developed to predict such complex functions is artificial neural networks (Cao et al. 2022). Artificial neural networks, developed by inspiring the working structure of the human brain, are tools that can learn functional relationships using input values and have the ability to predict target values in an output layer. The use of artificial neural networks can significantly reduce the time spent on numerical calculations (Wang et al. 2022). One of the most frequently used artificial neural network models is multi-layer perceptron (MLP) artificial neural network. MLP networks have input layer, output layer and at least one hidden layer. The hidden layer is located between the input and output layer. Each layer is connected to the next layer by a series of computing elements. The neuron located in the hidden layer has the basic function in the processing of the network and is characterized by bias (b), weight (w) and a transfer function (f). The neuron output is calculated using Eq. (2) with the appropriate transfer function (Ahmadloo and Azizi 2016):

$$Y_j = f\left(\sum_{i=1}^{n} W_{j,i}x_i + b_j\right) \tag{2}$$

Here Y is the neuron output, n is the number of neurons that connect to the jth neuron and x is the incoming signals. The process of learning the functional relationship between the data in the input layer and the target data of artificial neural networks is called "training". In the training phase, a training algorithm is used to minimize the error between input and target values. Bayesian training algorithm, which was first used by MacKay (1992) and Buntine and Weigend (1991), provides high predictive performance in artificial neural networks. In artificial neural networks developed with feed-forward back propagation, back propagation is made to the input layer in order to reduce the error rates obtained from the information feed-forward from the input layer. This process is terminated after the least error is reached (Feng et al. 2015). The basic flowchart of an artificial neural network is shown in Fig. 2.

In this study, an artificial neural network was developed in order to estimate the mercury values of the geoaccumulation index by using data from samples taken from 100

Table 1 Study area mercury concentration (ppm) and location

Sample no	Location	Hg	Sample no	Location	Hg	Sample no	Location	Hg
S1	Pasture	0.6	S8	Agricultural field	0.6	S15	Stream sediment	4.8
S2	Pasture	0.3	S9	Agricultural field	0.4	S16	Residential area	1.1
S3	Stream sediment	0.2	S10	Agricultural field	0.3	S17	Residential area	2.3
S4	Stream sediment	17.5	S11	Agricultural field	0.4	S18	Residential area	0.6
S5	Agricultural field	17.7	S12	Stream sediment	17.3	S19	Residential area	1.7
S6	Stream sediment	11.7	S13	Agricultural field	0.7	S20	Residential area	23.5
S7	Pasture	0.5	S14	Stream sediment	7.6	S21	Mine site	50.0

Table 2 Study area mercury concentration (ppm) and location

Sample no	Location	Hg	Sample no	Location	Hg	Sample no	Location	Hg
K_1	Agricultural field	3.4	K_4	Agricultural field	3.6	K_7	Highway railroad junction	8.8
	Agricultural field	2.8		Agricultural field	3.0		Highway railroad junction	9.2
	Agricultural field	8.2		Agricultural field	2.9		Highway railroad junction	7.7
K_2	Agricultural field	2.1	K_5	Agricultural field	0.9	K_8	Highway railroad junction	8.2
	Agricultural field	0.9		Agricultural field	1.1		Highway railroad junction	7.7
	Agricultural field	5.6		Agricultural field	1.1		Highway railroad junction	10.0
K_3	Agricultural field	0.9	K_6	Agricultural field	1.9	K_9	Agricultural field	1.0
	Agricultural field	2.2		Agricultural field	1.5		Agricultural field	1.0
	Agricultural field	2.3		Agricultural field	1.1		Agricultural field	0.8

Table 3 Study area mercury concentration (ppm) and location

Sample no	Location	Hg	Sample no	Location	Hg	Sample no	Location	Hg
D1	Stream sediment	2.1	T19	Agricultural field	0.6	T39	Agricultural field	0.6
D2	Stream sediment	1.1	T20	Agricultural field	0.5	T40	Agricultural field	0.9
T1	Agricultural field	2.6	T21	Agricultural field	0.6	T41	Agricultural field	0.4
T2	Agricultural field	1.0	T22	Agricultural field	0.5	U1	Residential area	0.9
T3	Agricultural field	0.9	T23	Agricultural field	2.0	U2	Residential area	0.6
T4	Agricultural field	0.7	T24	Agricultural field	1.8	U3	Residential area	0.8
T5	Agricultural field	0.5	T25	Agricultural field	2.2	U4	Residential area	0.4
T6	Agricultural field	0.6	T26	Agricultural field	1.5	U5	Residential area	1.3
T7	Agricultural field	0.4	T27	Agricultural field	1.1	U6	Residential area	0.8
T8	Agricultural field	0.9	T28	Highway railroad junction	5.0	U7	Residential area	2.1
T9	Agricultural field	0.5	T29	Highway railroad junction	1.8	U8	Residential area	2.4
T10	Agricultural field	0.6	T30	Residential area	1.8	U9	Residential area	3.0
T11	Agricultural field	0.8	T31	Residential area	1.4	U10	Residential area	1.5
T12	Agricultural field	0.9	T32	Residential area	0.4	U11	Residential area	1.0
T13	Agricultural field	0.7	T33	Residential area	0.4	U12	Residential area	1.0
T14	Agricultural field	0.8	T34	Residential area	0.6	U13	Residential area	0.8
T15	Agricultural field	0.6	T35	Highway railroad junction	6.0	U14	Residential area	0.4
T16	Agricultural field	0.5	T36	Highway railroad junction	5.0			
T17	Agricultural field	0.7	T37	Agricultural field	2.0			
T18	Agricultural field	0.8	T38	Agricultural field	1.0			

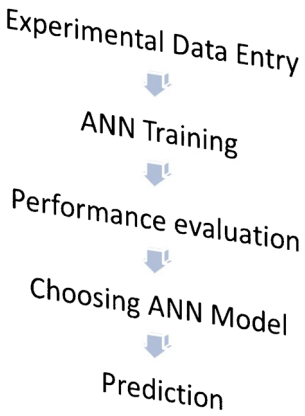

Fig. 2 Flowchart of the artificial neural network

different points. Optimizing the data used is extremely important in training of artificial neural networks (Çolak 2021). The data used in the training of multi-layer perceptron feed-forward back propagation artificial neural network is divided into two parts. Of the total data set, 90 (90%) were used for training of the neural network, and 10 (10%) were used for the testing phase. While the input parameters, which are the independent variables, were introduced to the MLP network, a numerical value definition was made for each of them, and the network model was entered in this way. In the artificial neural network developed using the Bayesian training algorithm and designed with 15 neurons in the hidden layer, five variable input layer data are defined, and the mercury values of the geoaccumulation index are estimated in the output layer. Hg was separated as the distance to the source of pollution, the source of the pollution, the characteristics of the sampling site and the primary factor controlling the movement. Hg was the element studied in this study. Pollution source, distance and characteristics of the sampled area, the areas where heavy metal accumulation occurs as a result of anthropogenically polluted or geogenic processes, the usage characteristics of these areas (pasture, settlement, agricultural area, etc.) are selected as parameters. The movement of Hg from the pollution source to the accumulation area was also determined as another parameter. The data used in the input layer of the artificial neural network are given in Table 4.

Table 4 Input parameters of the artificial neural network

Number	Definition
1	Hg (mercury)
2	Distance to pollution source
3	Source of pollution
4	Characteristics of the sampled place
5	The primary factor that controls moving

Tangent sigmoid (Tan-Sig) is used as the transfer function in the hidden layer of the artificial neural network, and the linear (Purelin) function is used as the transfer function in

the output layer. The functions of Tan-Sig and Purelin are given below (Zhou et al. 2021):

$$\mathrm{f}\left(net_j\right) = \frac{e^{net_j} - e^{-net_j}}{e^{net_j} + e^{-net_j}} \tag{3}$$

$$\mathrm{purelin(x)} = \mathrm{x} \tag{4}$$

The basic structure of the developed artificial neural network is shown in Fig. 3.

In order to evaluate the predictive performance of artificial neural networks, mean square error (MSE), R and margin of deviation (MoD) values were selected as criteria. MSE, R and MoD values are calculated using the equations given below (Çolak et al. 2020):

$$MSE = \frac{1}{N}\sum_{i=1}^{N}\left(I_{\mathrm{geo,exp}(i)} - I_{\mathrm{geo,ANN}(i)}\right)^2 \tag{5}$$

$$R = \sqrt{1 - \frac{\sum_{i=1}^{N}\left(I_{\mathrm{geo,exp}(i)} - I_{\mathrm{geo,ANN}(i)}\right)^2}{\sum_{i=1}^{N}\left(I_{\mathrm{geo,exp}(i)}\right)^2}} \tag{6}$$

$$MoD = \left[\frac{I_{\mathrm{geo,exp}} - I_{\mathrm{geo,ANN}}}{I_{\mathrm{geo,exp}}}\right] \times 100\% \tag{7}$$

where N is the number of data points, $I_{\mathrm{geo,ANN}}$ is the mercury values of the geoaccumulation index obtained from the artificial neural network model and $I_{\mathrm{geo,exp}}$ is the mercury values of the geoaccumulation index obtained experimentally.

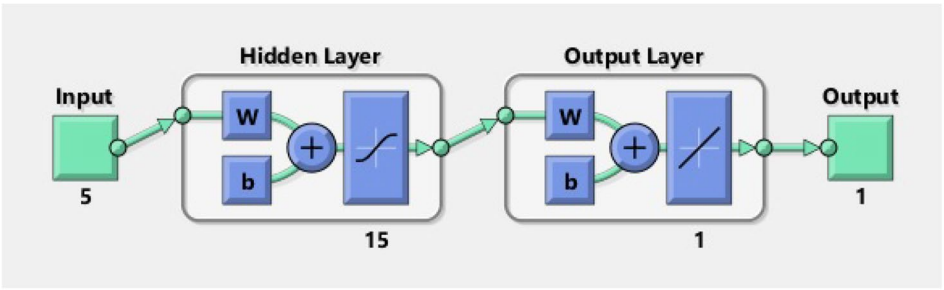

a)

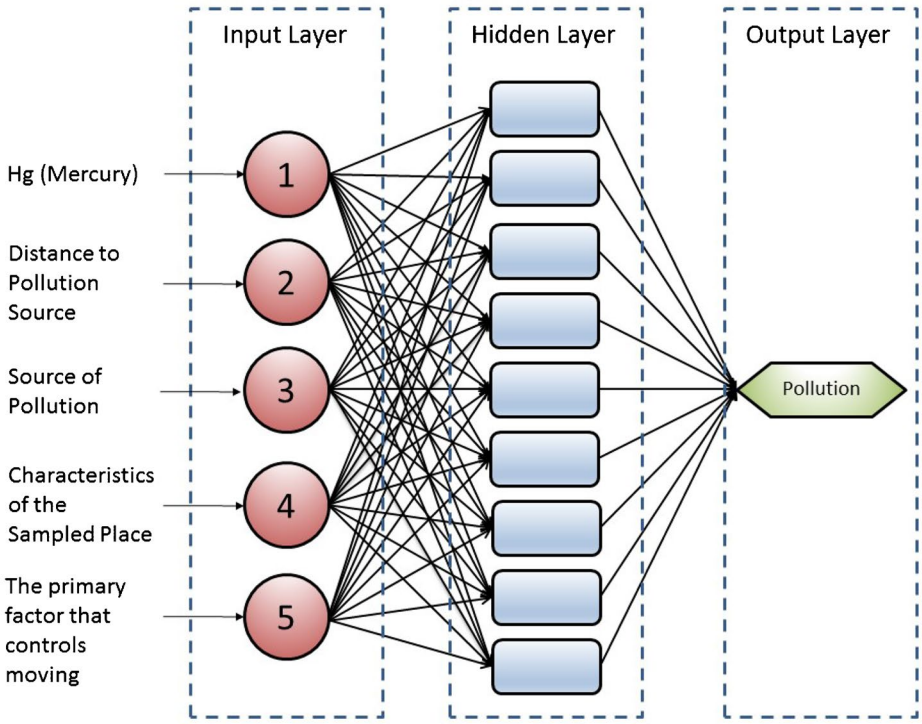

b)

Fig. 3 Properties of the artificial neural network. **a**) Main structure (from Matlab software) **b**) Topology

Result and discussion

In this study, the accumulation and distribution of mercury Fig. 4, which is a very dangerous metal for human health, in the soil were investigated by artificial intelligence model. Ladik is a settlement dating back to the Roman period, and mining activities in the region date back to ancient times. There is an accumulation of mercury in the region depending on the geological characteristics of the region and an accumulation due to human activities. This accumulation of mercury is of geogenic and anthropogenic origin. The geochemistry of these sediments is controlled by various factors such as geomorphological, hydrological, lithological and climatic events (Salomons and Förstner 1984). The accuracy of the training phase of the developed ANN model was examined. In Fig. 5, the change of MSE values in the training phase of the artificial neural network according to the epoch is given. As can be seen from the graphic, the MSE values, which were high at the beginning of the training phase of the artificial neural network, decreased in the following stages and reached the lowest value in the 86th epoch, and

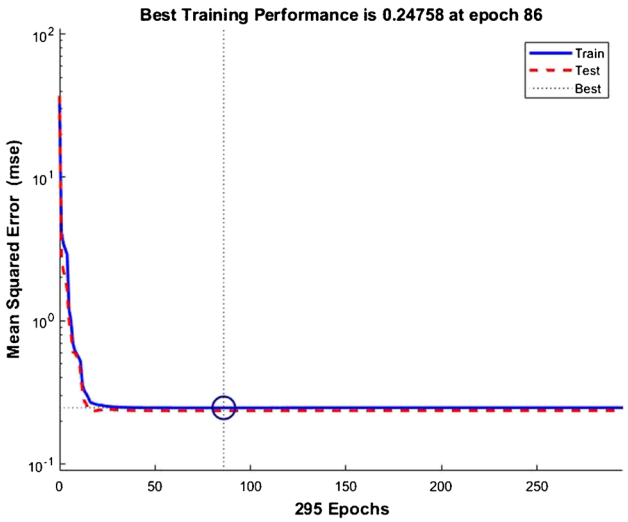

Fig. 5 Performance status according to MSE vs epoch

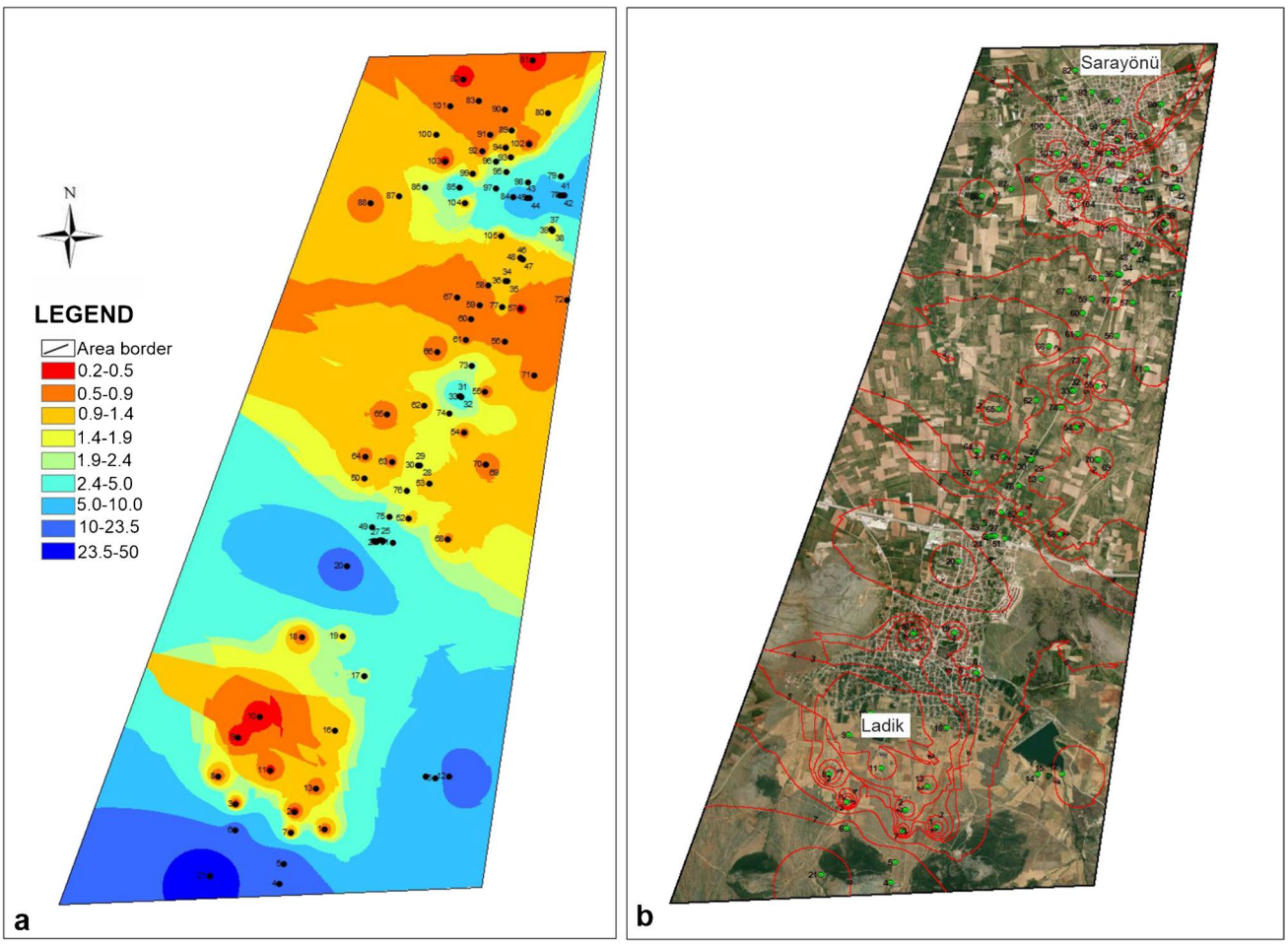

Fig. 4 Hg concentration distribution map

the training was ended by reaching the ideal stage. The point where the training line drawn in blue and the test line drawn in red intersect with the most ideal status line expressed in dotted line is the point where the training is terminated by minimizing the error values between the input and output layers of the artificial neural network. The MSE, which has high values at the beginning, decreases gradually and reaches the lowest value; however, the intersection of the training and test lines with the most ideal value line is the indicator that the training stage of the developed artificial neural network is ideally completed.

In Fig. 6, the error histogram graph of the developed artificial neural network is given. It is aimed to analyze the error rates of the artificial neural network better by displaying the error values obtained from the training and test phases of the artificial neural network in the error histogram graphs on the same graph. Considering the graph, it will be seen that the error rates in both stages of the artificial neural network are low around the zero error line,

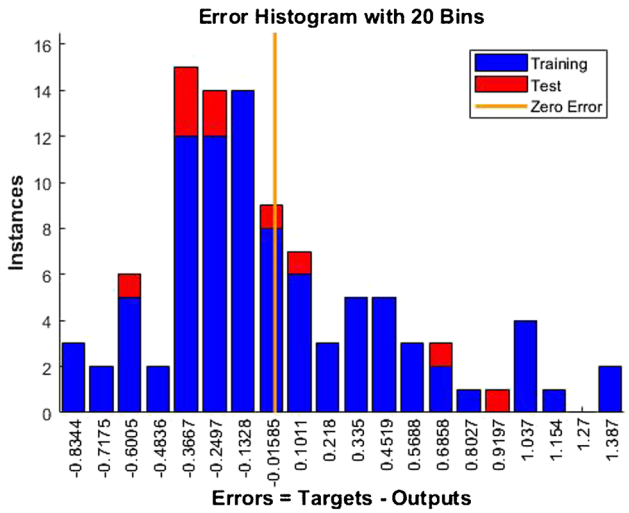

Fig. 6 Error histogram

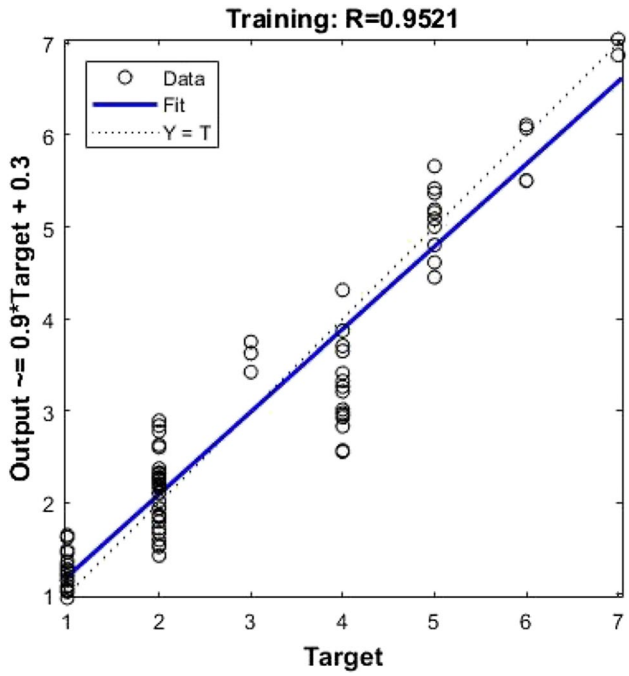

Fig. 7 Training performance of artificial neural network

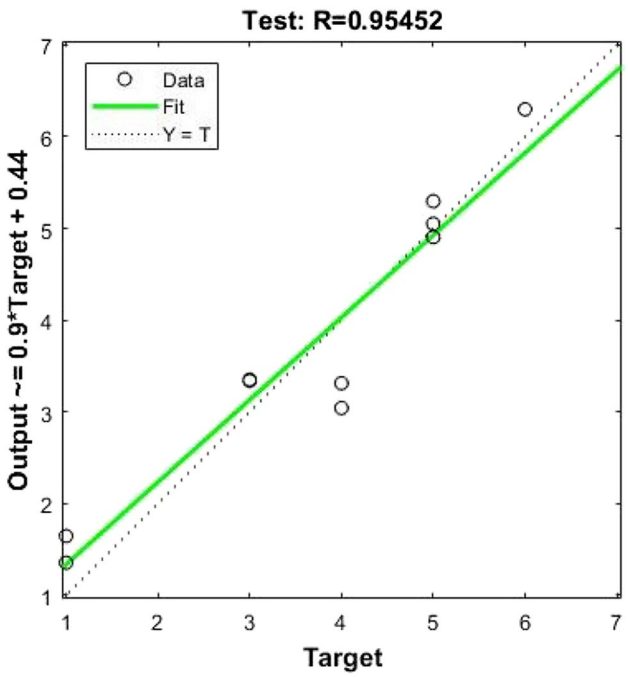

Fig. 8 Test performance of artificial neural network

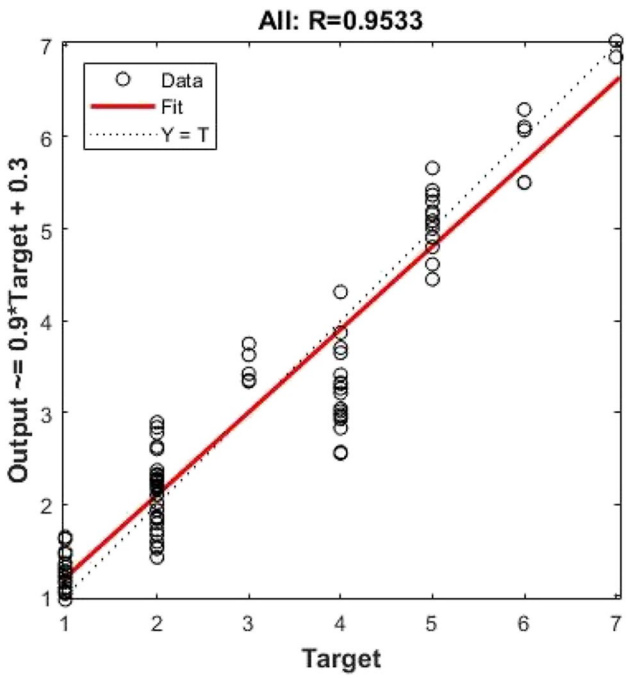

Fig. 9 General performance of artificial neural network

drawn in yellow, with the low error rates in the training and testing stages. These low values in error rates indicate that the artificial neural network is ideally designed and has predictive performance with acceptable error rates.

In Fig. 7, a comparison of the data obtained from the training phase of the artificial neural network with the experimental data is given. The fact that the data points are located around the equality line drawn in blue and that the *R* value is obtained as 0.9521 is an indication that the training stage of the artificial neural network is ideally completed and has a very low error rate.

Figure 8 shows the data obtained from the testing phase of the artificial neural network developed. The fact that the data points obtained from the test phase are located near the equality line drawn in green means that the testing phase of the artificial neural network is correctly terminated. However, the fact that the *R* value obtained for the test phase is 0.95452 indicates that the error rates of the test phase are at an acceptable level.

Figure 9 shows the performance graph of all data of the artificial neural network developed with a total of 100 data. It can be seen that all of the data points are located around the equality line drawn in red. For all data, *R* value was obtained as 0.9533. These results prove that the design phase of the artificial neural network is completed with an acceptable error rate. In Fig. 10, comparison of data obtained from artificial neural network and experimental data according to the number of data used from artificial neural network is given. While there are training, test and all data numbers on the x-axis of the graphs, there are mercury values of the geoaccumulation index on the y-axis. When the graphs shown separately according to training, test and all data are examined, it is seen that the data obtained from the artificial neural network overlap

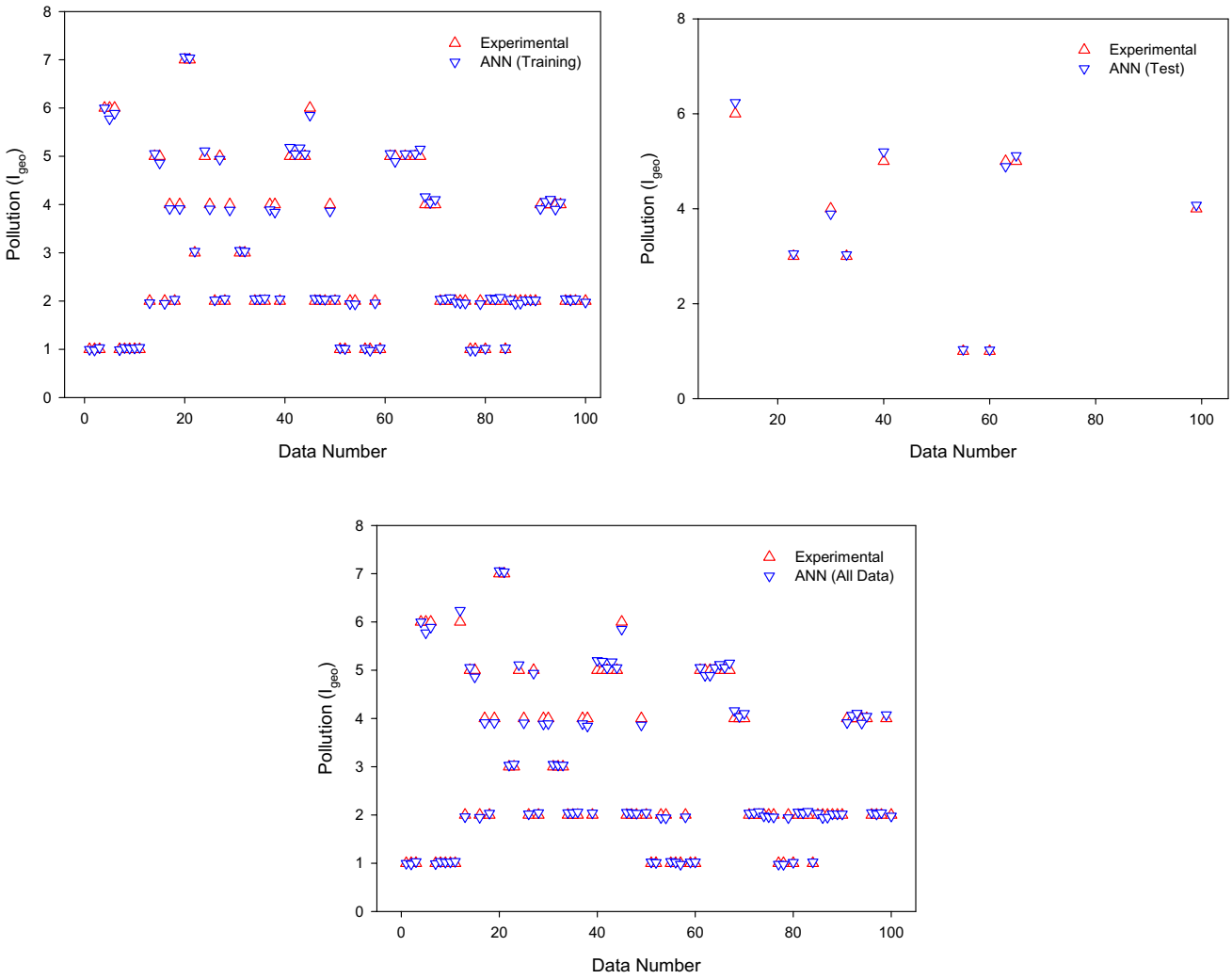

Fig. 10 Comparison of data obtained from artificial neural network and experimental data according to the number of data used for artificial neural network

with the experimental data. The minimal differences in position between the two points indicate that the designed artificial neural network can estimate the mercury values of the geoaccumulation index with an ideal and low error rate.

In Fig. 11, MoD values calculated with Eq. (7) are given. Investigation of MoD values is important in performance analysis of artificial neural networks. MoD values are numerical expressions of how much aberration the artificial neural network can estimate experimental data. Figure 11 shows the MoD values calculated for training, testing and all data of the artificial neural network. As can be seen from the graphic, MoD values are close to zero error line and low in all three stages. The results obtained for all the data of the artificial neural network showed that the developed artificial neural network can estimate the mercury values of the geoaccumulation index with an average error range of − 0.58%, ranging from − 4.04 to 3.98%. These low MoD values obtained prove that the developed artificial neural network has very high estimation performance and the margin of error is very low.

Data on the performance of the artificial neural network designed are given in Table 5. Considering the table, it is seen that MSE and MoD values are low and the *R* values obtained are very close to 1. The values given in Table 5 also confirm the high performance of the artificial neural network's predictive performance. In Fig. 12, the mercury values of the geoaccumulation index obtained from the artificial neural network with the experimental data are shown on the same graph. On the graph's x-axis are the mercury values for the geoaccumulation index that were determined experimentally, and on the y-axis are the outputs from artificial neural networks. It should be noted that the data points are located on the equality line drawn in red. This position of the data points is another proof that the developed neural network is designed to ideally predict the mercury values of the geoaccumulation index values with a minimum error rate.

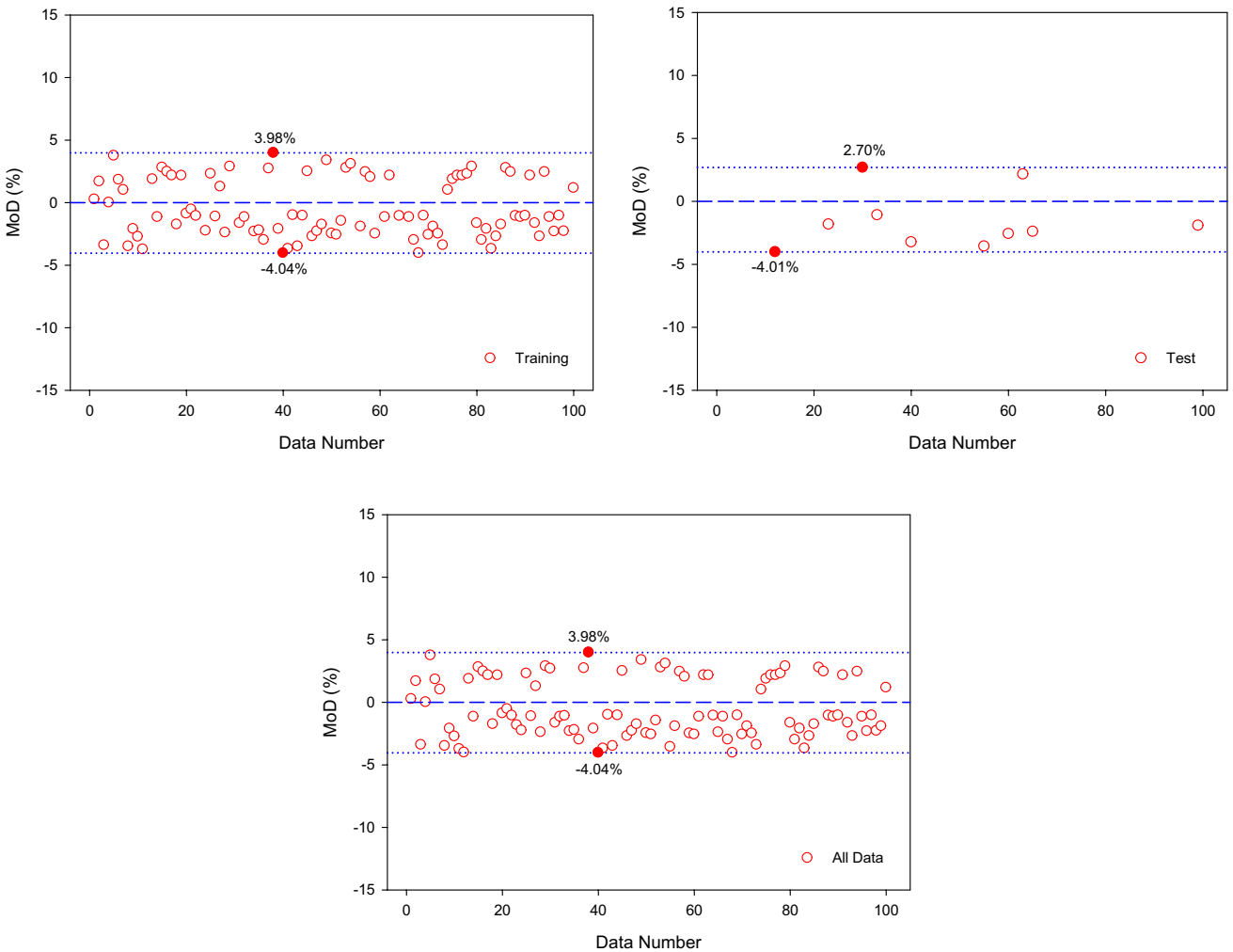

Fig. 11 MoD values of artificial neural network developed

Table 5 Performance values of the artificial neural network

	MSE	R	MoD
Training	2.38×10^{-1}	0.9521	−0.47
Test	1.81×10^{-1}	0.95452	−1.65
All	2.10×10^{-1}	0.9533	−0.58

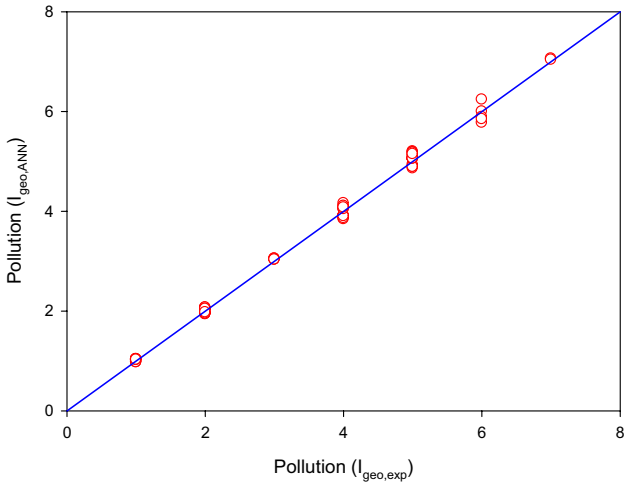

Fig. 12 Data obtained from the artificial neural network vs the experimental data

Conclusion

It is crucial that environmental effect characteristics can be predicted with accuracy without the need of time-consuming, expensive experiments. In this study, an ANN model is proposed in order to predict the pollution analysis of the Ladik-Sarayönü region. Five variables were defined in the input layer of the network model designed using MLP architecture, and mercury values in the output layer were obtained. Mercury values are considered an important phenomenon in environmental pollution impact assessment. Bayesian training algorithm was used in the ANN model designed with 15 neurons in the hidden layer. In the development of the ANN model, a total of 103 data sets obtained from the mercury concentrations of the samples taken from the field were used. The data obtained from the literature were used in grouping the data set used in the development of the model. The obtained results showed that if developed, the ANN model could predict the mercury values of the geoaccumulation index value with an average error of 0.58%. In the future, studies can be conducted to make pollution estimations of different regions with different parameters.

Data Availability Data will be available from authors upon reasonable request.

Declarations

Conflict of interest The authors declare no competing interests.

References

Ahmadloo E, Azizi S (2016) Prediction of thermal conductivity of various nanofluids using artificial neural network. Int Commun Heat Mass Transfer 74:69–75. https://doi.org/10.1016/j.icheatmasstransfer.2016.03.008

Akinpelu AA, Ali ME, Owolabi TO, Johan MR, Saidur R, Olatunji SO, Chowdbury Z (2020) A support vector regression model for the prediction of total polyaromatic hydrocarbons in soil: an artificial intelligent system for mapping environmental pollution. Neural Comput Applic 32:14899–14908. https://doi.org/10.1007/s00521-020-04845-3

Bahiraei M, Heshmatian V, Moayedi V (2019) Artificial intelligence in the field of nanofluids: a review on applications and potential future directions. Powder Technol 353:276–301. https://doi.org/10.1016/j.powtec.2019.05.034

Bazoobandi A, Emamgholizadeh S, Ghorbani H (2019) Estimating the amount of cadmium and lead in the polluted soil using artificial intelligence models. Eur J Environ Civ Eng. https://doi.org/10.1080/19648189.2019.1686429

Buntine WL, Weigend AS (1991) Bayesian back-propagation. Complex Syst 5:603–643

Cao Y, Kamrani E, Mirzaei S, Khandakar A, Vaferi B (2022) Electrical efficiency of the photovoltaic/thermal collectors cooled by nanofluids: machine learning simulation and optimization by evolutionary algorithm. Energy Rep 8:24–36. https://doi.org/10.1016/j.egyr.2021.11.252

Cheng HX, Zhao CD, Liu F, Yang K (2013) Mercury drop trend in urban soils in Beijing, China, since 1987. J Geochem Explor 124:195–202. https://doi.org/10.1016/j.gexplo.2012.09.007

Çolak AB (2021) An experimental study on the comparative analysis of the effect of the number of data on the error rates of artificial neural networks. Int J Energy Res 45:478–500. https://doi.org/10.1002/er.5680

Çolak AB, Yıldız O, Bayrak M, Tezekici BS (2020) Experimental study for predicting the specific heat of water based Cu-Al_2O_3 hybrid nanofluid using artificial neural network and proposing new correlation. Int J Energy Res 44:7198–7215. https://doi.org/10.1002/er.5417

Coskun A, Horasan BY, Ozturk A (2021) Heavy metal distribution in stream sediments and potential ecological risk assessment in Konya Northeast region. Environ Earth Sci 80:181. https://doi.org/10.1007/s12665-021-09495-9

Emamgholizadeh S, Esmaeilbeiki F, Babak M, Zarehaghi D, Maroufpoor E, Rezaei H (2018) Communications in soil science and plant analysis estimation of the organic carbon content by the pattern recognition method. Commun Soil Sci Plant Anal 49(17):2143–2154. https://doi.org/10.1080/00103624.2018.1499750

Feng Q, Zhang J, Zhang X, Wen S (2015) Proximate analysis based prediction of gross calorific value of coals: a comparison of support vector machine, alternating conditional expectation and artificial neural network, Fuel Process. Technol 129:120–129. https://doi.org/10.1016/j.fuproc.2014.09.001

Fu XW, Zhang H, Wang X, Yu B, Lin CJ, Feng XB (2015) Observations of at mospheric mercury in China: a critical review. Atmos

Chem Phys Discuss 15:9455–9476. https://doi.org/10.5194/acp-15-9455-2015
Gall JE, Boyd RS, Rajakaruna N (2015) Transfer of heavy metals through terrestrial food webs: a review. Environ Monit Assess 187:201. https://doi.org/10.1007/s10661-015-4436-3
Gao W, Guirao JLG, Basavanagoud B, Wu J (2018) Partial multi-dividing ontology learning algorithm. Inf Sci 467:35–58. https://doi.org/10.1016/j.ins.2018.07.049
Gao W, Dimitrov D, Abdo H (2019) Tight independent set neighborhood union condition for fractional critical deleted graphs and ID deleted graphs. Dis Cont Dyn Syst-S 12:711–721. https://doi.org/10.3934/dcdss.2019045
Horasan BY, Ozturk A, Unal Y (2020) Geochemical and anthoropogenic factors controling the heavy metal accumulation in the soils of Sarayonu Ladık Link Roads. Carpathian J Earth Environ Sci 15:145–156. https://doi.org/10.26471/cjees/2020/015/117
Khalil A, Hanich L, Bannari A, Zouhri L, Pourret O, Hakkou R (2013) Assessment of soil contamination around an abandoned mine in a semi-arid environment using geochemistry and geostatistics: prework of geochemical process modeling with numerical models. J Geochemical Explor 125:117–129. https://doi.org/10.1016/j.gexplo.2012.11.018
Kim KH, Lindberg SE (1995) Design and initial tests of a dynamic enclosure chamber for measurements of vapor-phase mercury fluxes over soils. Water, Air, Soil Pollut 80:1059–1068. https://doi.org/10.1007/978-94-011-0153-0_120
MacKay DJ (1992) A practical Bayesian framework for backpropagation networks. Neural Comput 4:448–472. https://doi.org/10.1162/neco.1992.4.3.448
Manwani S, Vanisree CR, Jaiman V, Awasthi KK, Yadav CS, Sankhla MS, Pandit PP, Awasthi G (2022) Heavy metal contamination in vegetables and their toxic effects on human health, ın sustainable crop production: recent advances, edited by Vijay Meena et al, IntechOpen, London. https://doi.org/10.5772/intechopen.102651
Moosavi SR, Vaferi B, Wood DA (2012) Auto-characterization of naturally fractured reservoirs drilled by horizontal well using multi-output least squares support vector regression. Arab J Geosci 14:545. https://doi.org/10.1007/s12517-021-06559-9
Muller G (1969) Index of geoaccumulation in sediments of the Rhine River. GeoJournal 2:108–118
Nourani V, Gökçekuş H, Umar IK (2020) Artificial intelligence based ensemble model for prediction of vehicular traffic noise. Environ Res 180:108852. https://doi.org/10.1016/j.envres.2019.108852
Ozturk A, Arici OK (2021) Carcinogenic-potential ecological risk assessment of soils and wheat in the eastern region of Konya (Turkey). Environ Sci Pollut Res 28:15471–15484. https://doi.org/10.1007/s11356-020-11697-w
Salomons W, Förstner U (1984) Metals in the hydrocycle. Springer-Verlag, Berlin
Sierra MJ, López-Nicolás R, González-Bermúdez C, Frontela C, Saseta C, Millán R (2017) Cultivation of Solanum tuberosum in a former mining district for a safe human consumption integrating simulated digestion. J Sci Food Agric 97(15):5278–5286. https://doi.org/10.1002/jsfa.8412
Solgun E, Horasan BY, Ozturk A (2021) Heavy metal accumulation and potential ecological risk assessment in sediments from the southwestern Konya district (Turkey). Arab J Geosci 14:730. https://doi.org/10.1007/s12517-021-07088-1
Srinivasa GS, Reddy MR, Govil PK (2019) Assessment of heavy metal contamination in soils at Jajmau (Kanpur) and Unnao industrial areas of the Ganga plain, Uttar Pradesh, India. Hazard Mat 174:113–121. https://doi.org/10.1016/j.jhazmat.2009.09.024
Tiodar Emanuela D, Văcar CL, Dorina P (2021) Phytoremediation and microorganisms-assisted phytoremediation of mercury-contaminated soils: challenges and perspectives. Int J Environ Res Public Health 18(5):2435. https://doi.org/10.3390/ijerph18052435
Tóth G, Hermann T, Da Silva MR, Montanarella L (2016) Heavy metals in agricultural soils of the European Union with implications for food safety. Environ Int 88:299–309. https://doi.org/10.1016/j.envint.2015.12.017
Wang J, Ayari MA, Khandakar A, Chowdhury MEH, Uz Zaman SM, Rahman T, Vaferi B (2022) Estimating the relative crystallinity of biodegradable polylactic acid and polyglycolide polymer composites by machine learning methodologies. Polymers 14:527. https://doi.org/10.3390/polym14030527
Zhou Z, Davoudi E, Vaferi B (2021) Monitoring the effect of surface functionalization on the CO_2 capture by graphene oxide/methyl diethanolamine nanofluids. J Environ Chem Eng 9:106202. https://doi.org/10.1016/j.jece.2021.106202